Dynamical coupled channels calculation of pion and omega meson production

Mark W. Paris*

Excited Baryon Analysis Center, Thomas Jefferson National Accelerator Facility, 12000 Jefferson Avenue MS12H2 Newport News, Virginia 23606, USA

(Received 22 February 2008; revised manuscript received 19 November 2008; published 26 February 2009)

The dynamical coupled-channels approach developed at the Excited Baryon Analysis Center is extended to include the ωN channel to study π- and ω-meson production induced by scattering pions and photons from the proton. Six intermediate channels, including πN, ηN, $\pi\Delta$, σN, ρN, and ωN, are employed to describe unpolarized and polarized data. Bare parameters in an effective hadronic Lagrangian are determined in a fit to the data for $\pi N \to \pi N$, $\gamma N \to \pi N$, $\pi^- p \to \omega n$, and $\gamma p \to \omega p$ reactions at center-of-mass energies from threshold to $W < 2.0$ GeV. The T matrix determined in these fits is used to calculate the photon beam asymmetry for ω-meson production and the $\omega N \to \omega N$ total cross section and ωN-scattering lengths. The calculated beam asymmetry is in good agreement with the observed in the range of energies near threshold to $W \lesssim 2.0$ GeV.

DOI: 10.1103/PhysRevC.79.025208 PACS number(s): 13.60.Le, 11.80.Gw, 13.75.Gx, 24.10.Eq

I. INTRODUCTION

The present work is an extension of dynamical coupled-channels method developed by Matsuyama, Sato, and Lee [1] to include the contribution of the ωN channel. Calculations presented here form part of an ongoing program of analysis of electromagnetic meson production data at the Excited Baryon Analysis Center housed at the Thomas Jefferson National Accelerator Facility, the central purpose of which is the extraction from data of the properties of resonant excitations of the nucleon and their interpretation.

Nucleon resonances are thought to play a decisive role in reactions of strong, electromagnetic and weak probes on nucleons at energies $W < 2.0$ GeV. The extent to which nucleon resonances determine unpolarized and polarized observables in meson production reactions and the role of nonresonant contributions in these reactions remains an open question in this energy region. Model determinations of the T matrix consistent with the observed meson production data in this kinematic regime seek to resolve the resonance spectrum of the nucleon. Such a determination is useful to gain insight into fundamental aspects of quantum chromodynamics such as the role of chiral symmetry and confinement and a detailed understanding of the correlations among the strongly interacting quarks.

The amount of experimental data for the ω-meson production reaction in the resonance region is rapidly increasing. There is existing high-precision data from the SAPHIR Collaboration [2] for the $\gamma p \to \omega p$ reaction from which the unpolarized differential cross section (DCS) and decay angular distributions have been extracted. Consistent with this data are the more recent measurements of the GRAAL Collaboration [3,4]. More photoproduction data at similar kinematics is anticipated from the CLAS Collaboration [5]. The $\pi N \to \omega N$ data from bubble and drift chamber experiments is of low precision and there is little overlap in different experiment's [6,7] kinematics. Though there is some discussion in the literature about the validity of the extracted cross sections [8,9] we assume the data are correct as originally published.

The importance of including off-shell effects in dynamical coupled-channels formulations of strong and electromagnetic meson production reactions has been extensively studied [10,11]. The present study incorporates off-shell effects in a coupled-channels approach and is comparable to the model treatments of Krehl *et al.* [11] and Chen *et al.* [12]. It should be contrasted with coupled-channels calculations that take into account coupling of the intermediate states only to the continuum and neglect their off-shell contributions such as those of the Giessen group [13] and KVI [14]. In the Giessen study, an effective Lagrangian is adopted for the channels πN, $\pi\pi N$, ηN, ωN, $K\Lambda$, and $K\Sigma$. They assume a resonant contribution similar to the one adopted in the present study.

Motivations for studying the ωN reaction are manifold. Aside from insight into the $T = \frac{1}{2}$ resonance spectrum and implications for meson production reactions, the vector mesons are thought to be important components in very dense matter in the neutron-rich stellar environment [15–17]. In nuclear matter, the ωNN coupling can play a significant role in determining the equation of state in some models [18].

The present hadronic dynamical model has about 500 parameters. The nonresonant terms include bare hadron masses, couplings, and cutoffs and the resonant terms include bare resonance masses, couplings, and cutoffs in each of six channels and 14 partial waves and 17 resonances. We determine the T matrix via fits to a large subset ($\sim$1800 data points) of the available data in several reaction channels (described in detail in Sec. III) by varying the parameters (masses, couplings, etc.) of the model. The T matrix determined in this way is used to calculate the photon beam asymmetry for ω-meson production (not included in the fit data) shown in Fig. 15. The good quality of the agreement of the resulting calculated beam asymmetry with the observed data [4] suggests that the present values of the parameters are stable to increases in the fit data set. It is hoped that the present model incorporates dynamics sufficient

*Present address: Center for Nuclear Studies, Data Analysis Center, George Washington University, 20101 Academic Way, Ashburn, Virginia 20147; mparis@gwu.edu.

for a realistic description of the meson production data in the explored channels for the given range of energies.

In the next section we briefly describe the model theory for the six-channel model. The results of the fit to the data are presented and discussed in Sec. III. The final section gives conclusions and descriptions for improvements to the present study that are under development.

II. MODEL REACTION THEORY

The T matrix for $\pi N \to MB$ and $\gamma N \to MB$ (in this work the final MB state is restricted to $\pi N, \omega N$) is written as a sum of nonresonant, t and resonant, t^R contributions

$$T(E) = t(E) + t^R(E), \tag{1}$$

where $E = W$ is the scattering energy of the particles in the center-of-mass frame. Qualitatively, the nonresonant contribution includes rescattering and coupled-channels effects on the Born amplitudes while the resonant contribution includes these effects for the resonance transition form factors and the resonance propagators. No assumption is made about the relative size of the contributions of these terms. Our first objective in this work is to determine the $T(E)$ in fits to the observed data.

Except for the $\pi N \to \pi N$ reaction where we fit to the energy-dependent solution for the partial wave amplitudes of Arndt *et al.* [19], we fit unpolarized and polarized cross sections of the γ- and π-induced reactions. The DCS for π-induced reactions is related to the T matrix as

$$\frac{d\sigma_\pi}{d\Omega} = \frac{(4\pi)^2}{k^2}\rho_{M'N'}(k')\rho_{\pi N}(k) \times \frac{1}{2}\sum_{M_{M'},M_{N'}}\sum_{M_N}|T_{M_{M'}M_{N'},M_N}(\mathbf{k}',\mathbf{k};E)|^2, \tag{2}$$

where $\mathbf{k}$ is the relative momentum of the initial πN state and $\mathbf{k}'$ is the relative momentum of the final meson-nucleon ($M'N'$) state, where $M' = \pi$ or ω. The spin projection of the particles in the inital (final) state is M_N ($M_{M'}$, $M_{N'}$). The quantity $\rho_{MB}(p) = \frac{\pi p E_M(p) E_B(p)}{E_M(p)+E_B(p)}$, where $E_i(p) = \sqrt{p^2 + m_i^2}$ is related to the density of states. A similar relation holds for the unpolarized photoproduction cross section $\frac{d\sigma_\gamma}{d\Omega}$.

A. Nonresonant contribution

The nonresonant contribution to the transition matrix in the partial-wave representation for the pion-induced $t^{JT}_{L'S'M'N',\ell\pi N}(E)$ and the mixed partial-wave/helicity representation for the photon-induced $t^{JT}_{L'S'M'N',\lambda_\gamma\lambda_N T_{N,z}}(E)$ reactions are

$$\begin{aligned} t^{JT}_{L'S'M'N',\ell\pi N}(k',k;E) &= v^{JT}_{L'S'M'N',\ell\pi N}(k',k) \\ &\quad + \sum_{LSMB}\int_0^\infty dp\, p^2 t^{JT}_{L'S'M'N',LSMB}(k',p;E) \\ &\quad \times G_{0,MB}(p;E) v^{JT}_{LSMB,\ell\pi N}(p,k), \end{aligned} \tag{3}$$

$$\begin{aligned} t^{JT}_{L'S'M'N',\lambda_\gamma\lambda_N T_{N,z}}(k,q;E) &= v^{JT}_{L'S'M'N',\lambda_\gamma\lambda_N T_{N,z}}(k,q) \\ &\quad + \sum_{LSMB}\int_0^\infty dp\, p^2 t^{JT}_{L'S'M'N',LSMB}(k,p;E) \\ &\quad \times G_{0,MB}(p;E) v^{JT}_{LSMB,\lambda_\gamma\lambda_N T_{N,z}}(p,q), \end{aligned} \tag{4}$$

where T is the total isospin and $T_{N,z}$ is the isospin projection of the nucleon in the initial state, J is the total angular momentum of the partial wave, $L(L')$ is the partial wave orbital angular momentum of the intermediate (final) state, $S(S')$ is the total intrinsic spin of the particles in the intermediate (final) state, and $\ell = J \pm \frac{1}{2}$ is the πN initial state orbital angular momentum. The included partial waves are shown in Table I. Channels are defined by the meson species $M'(M)$ of the final (intermediate) state and $N(N')$, the nucleon of the initial(final) state or B, the intermediate state baryon associated with the meson M of channel MB. The sums, $\sum_{MB}$ are over channels

TABLE I. The (L, S) terms for partial waves ℓ_{TJ} for included channels.

ℓ_{TJ}	πN	ηN	$\pi\Delta$	σN	ρN	ωN
S_{11}	$(0,\frac{1}{2})$	$(0,\frac{1}{2})$	$(2,\frac{3}{2})$	$(1,\frac{1}{2})$	$(0,\frac{1}{2})$ $(2,\frac{3}{2})$	$(0,\frac{1}{2})$ $(2,\frac{3}{2})$
S_{31}	$(0,\frac{1}{2})$		$(2,\frac{3}{2})$		$(0,\frac{1}{2})$ $(2,\frac{3}{2})$	
P_{11}	$(1,\frac{1}{2})$	$(1,\frac{1}{2})$	$(1,\frac{3}{2})$	$(0,\frac{1}{2})$	$(1,\frac{1}{2})$ $(1,\frac{3}{2})$	$(1,\frac{1}{2})$ $(1,\frac{3}{2})$
P_{13}	$(1,\frac{1}{2})$	$(1,\frac{1}{2})$	$(1,\frac{3}{2})$ $(3,\frac{3}{2})$	$(2,\frac{1}{2})$	$(1,\frac{1}{2})$ $(1,\frac{3}{2})$ $(3,\frac{3}{2})$	$(1,\frac{1}{2})$ $(1,\frac{3}{2})$ $(3,\frac{3}{2})$
P_{31}	$(1,\frac{1}{2})$		$(1,\frac{3}{2})$		$(1,\frac{1}{2})$ $(1,\frac{3}{2})$	
P_{33}	$(1,\frac{1}{2})$		$(1,\frac{3}{2})$ $(3,\frac{3}{2})$		$(1,\frac{1}{2})$ $(1,\frac{3}{2})$ $(3,\frac{3}{2})$	
D_{13}	$(2,\frac{1}{2})$	$(2,\frac{1}{2})$	$(0,\frac{3}{2})$ $(2,\frac{3}{2})$	$(1,\frac{1}{2})$	$(2,\frac{1}{2})$ $(0,\frac{3}{2})$ $(4,\frac{3}{2})$	$(2,\frac{1}{2})$ $(0,\frac{3}{2})$ $(2,\frac{3}{2})$
D_{15}	$(2,\frac{1}{2})$	$(2,\frac{1}{2})$	$(2,\frac{3}{2})$ $(4,\frac{3}{2})$	$(3,\frac{1}{2})$	$(2,\frac{1}{2})$ $(2,\frac{3}{2})$ $(4,\frac{3}{2})$	$(2,\frac{1}{2})$ $(2,\frac{3}{2})$ $(4,\frac{3}{2})$
D_{33}	$(2,\frac{1}{2})$		$(0,\frac{3}{2})$ $(2,\frac{3}{2})$		$(2,\frac{1}{2})$ $(0,\frac{3}{2})$ $(2,\frac{3}{2})$	
D_{35}	$(2,\frac{1}{2})$		$(2,\frac{3}{2})$ $(4,\frac{3}{2})$		$(2,\frac{1}{2})$ $(2,\frac{3}{2})$ $(4,\frac{3}{2})$	
F_{15}	$(3,\frac{1}{2})$	$(3,\frac{1}{2})$	$(1,\frac{3}{2})$ $(3,\frac{3}{2})$	$(2,\frac{1}{2})$	$(3,\frac{1}{2})$ $(1,\frac{3}{2})$ $(3,\frac{3}{2})$	$(3,\frac{1}{2})$ $(1,\frac{3}{2})$ $(3,\frac{3}{2})$
F_{17}	$(3,\frac{1}{2})$	$(3,\frac{1}{2})$	$(3,\frac{3}{2})$ $(5,\frac{3}{2})$	$(4,\frac{1}{2})$	$(3,\frac{1}{2})$ $(3,\frac{3}{2})$ $(5,\frac{3}{2})$	$(3,\frac{1}{2})$ $(3,\frac{3}{2})$ $(5,\frac{3}{2})$
F_{35}	$(3,\frac{1}{2})$		$(1,\frac{3}{2})$ $(3,\frac{3}{2})$		$(3,\frac{1}{2})$ $(1,\frac{3}{2})$ $(3,\frac{3}{2})$	
F_{37}	$(3,\frac{1}{2})$		$(3,\frac{3}{2})$ $(5,\frac{3}{2})$		$(3,\frac{1}{2})$ $(3,\frac{3}{2})$ $(5,\frac{3}{2})$	

TABLE II. Propagator masses (MeV) appearing in Eq. (5).

m_N	938.5
m_π	138.5
m_η	547.5
m_Δ	1300.0
m_σ	898.6
m_ρ	811.7
m_ω	782.6

πN, ηN, $\pi\Delta$, σN, ρN, and ωN. Here $G_{0,MB}(p;E)$ is the relativistic free particle Green's function

$$G_{0,MB}(p;E) = \frac{1}{E - E_M(p) - E_B(p) - \Sigma_{MB}(p;E)}. \quad (5)$$

$E_i(p)$ are the free particle energies with masses given in Table II and $\Sigma_{MB}(p;E)$ is the self-energy of the unstable particle in channels $MB = \pi\Delta, \sigma N, \rho N$, including the effects induced by the decay of the unstable particle in these channels [1]. Channels with stable particles $MB = \pi N, \eta N, \omega N$ have $\Sigma_{MB} = -i\epsilon$ corresponding to the coupling to on-shell intermediate states. The width of the ω meson $\Gamma_\omega = 8.5(1)$ MeV is neglected.

The $v_{M'B',MB}$ and $v_{MB,\gamma N}$ are the effective nonresonant interaction Hamiltonians for hadrons $\pi, \eta, \sigma, \rho, \omega, N, \Delta$, and photons, γ. These interactions are Born amplitudes derived from the Lagrangian of Ref. [1] and subjected to the unitary transformation method of Ref. [20]. It yields an interaction that is independent of the scattering energy, $E = W$, and depends only on the relative three-momenta of the incoming and outgoing particles.

In the present model there are 74 interaction mechanisms among the channels πN, ηN, $\pi\Delta$, σN, ρN, ωN, and γN. Figures 1–4 show examples of these explicitly for the terms involving γN, πN, and ωN channels for pion-induced and photoproduction amplitudes. In this work we neglect the contribution of the high-mass a_J and f_J mesons [except the $f_0/\sigma(600)$]. We make the further simplification in the nonresonant hadronic interaction involving the ωN channel of

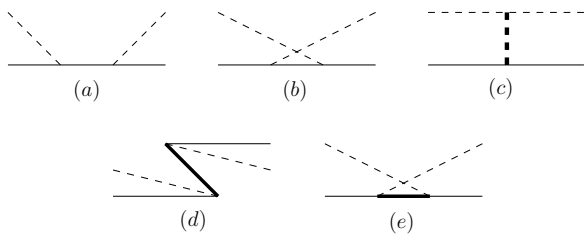

FIG. 1. The interactions $v_{M'B',MB}$ and $v_{MB,\gamma N}$ include 74 interaction mechanisms. In this figure and Figs. 2, 3, and 4 we show a subset of these. Here the $v_{\pi N,\pi N}$ interaction mechanisms are shown. The nucleon is denoted by a thin, solid line, the pion by a thin, dashed line, the ρ meson by a thick, dashed line, and the Δ by a thick solid line. (a) s-channel nucleon exchange; (b) u-channel nucleon exchange; (c) t-channel ρ exchange; (d) s-channel $\bar{\Delta}$ exchange; (e) u-channel Δ exchange.

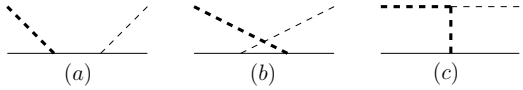

FIG. 2. The $v_{\omega N,\pi N}$ interaction mechanisms. (a) s-channel nucleon exchange; (b) u-channel nucleon exchange; (c) t-channel ρ exchange.

including only those terms which couple the ωN to itself and to πN, that is: $v_{\omega N,MB} = v_{\omega N,\pi N}\delta_{\pi N,MB} + v_{\omega N,\omega N}\delta_{\omega N,MB}$. This simplification permits the introduction of a minimal number of additional bare parameters for the ωN channel while retaining effects from each of the nonresonant s, t, and u mechanisms. In this way, we include the behavior associated with each mechanism while maintaining a tractable model.

Equations (3) and (4) represent the bulk of the computational effort required to carry out the coupled-channels dynamical approach (at the two-body level). Most of the computer time required ($\sim$3/5) is spent evaluating the Born terms. Much of the remainder is spent inverting the matrix representing the scattering wave function, $\mathcal{F}^{-1} = (1 - vG_0)^{-1} = 1 + tG_0$ appearing in Eq. (3) on a momentum grid of 25 *Gauss-Legendre* points using standard subtraction methods [21]. Convergence has been checked with grids of up to 45 GL points. A parallel FORTRAN90 code has been developed to cope with the long evaluation times for a single χ^2 evaluation ($\sim$100 node·m). It exploits the independence of the partial waves and energies in the evaluation of the T matrix. Typically $\sim 10^3$–10^4 χ^2 evaluations are required for optimization using the MINUIT package [22].

The amplitudes $t^{JT}_{LSMB,\ell\pi N}$ include partial-wave contributions up to and including $L = 3$ (F wave). The same is true for the electromagnetic terms except for the t-channel pion exchange in Fig. 4(i). In this case, all partial waves are required for convergence. For $L > 3$ the contribution to the electromagnetic nonresonant amplitude $t^{JT}_{L'S'M'N',\lambda_\gamma\lambda_N T_{N,z}}(k,q;E)$ is calculated at the Born amplitude level only and neglects the effects due to final-state interactions and coupled channels, i.e., the second terms of Eq. (4).

The nonresonant interaction depends on the masses of the hadrons and their coupling and cutoff parameters. These values obtained in the five-channel fit of Ref. [1] are shown here in Tables III and IV for completeness. For the interaction terms, $v_{M'B',MB}$ and $v_{MB,\gamma N}$ [other than the mass of $f_0/\sigma(600)$ which is a fit parameter], the physical particle masses are used. Form factors are included at vertices in the nonresonant interactions, $v_{M'B',MB}$ and $v_{MB,\gamma N}$ have the form $F(|\mathbf{q}|;m) = [\Lambda^2/(\Lambda^2 + |\mathbf{q}|^2)]^m$. Here $|\mathbf{q}|$ is either the momentum transferred at the vertex or the relative momentum [23]. We use the value $m = 2$ at all vertices.

FIG. 3. The $v_{\omega N,\omega N}$ interaction mechanisms. (a) s-channel nucleon exchange; (b) u-channel nucleon exchange.

TABLE III. Lagrangian bare coupling and σ mass.

$f^2_{\pi NN}/4\pi$	0.08
$f_{\pi N\Delta}$	2.206
$f_{\eta NN}$	3.889
$g_{\rho NN}$	8.721
κ_ρ	2.654
$g_{\omega NN}$	8.100
κ_ω	1.020
$g^t_{\omega NN}$	1.298
κ^t_ω	1.002
$g_{\sigma NN}$	6.815
$g_{\rho\pi\pi}$	4.000
$f_{\pi\Delta\Delta}$	1.000
$f_{\rho N\Delta}$	7.516
$g_{\sigma\pi\pi}$	2.353
$g_{\omega\pi\rho}$	6.956
$g_{\rho\Delta\Delta}$	3.302
$\kappa_{\rho\Delta\Delta}$	2.000
$g_{\rho\pi\gamma}$	$0.1027e$
$g_{\omega\pi\gamma}$	$0.3247e$
m_σ	500.1 MeV

B. Resonant contribution

The resonant contribution, $t^R(E)$ to the T matrix is given as

$$t^{R,JT}_{LSMB,\ell\pi N}(k',k;E) = \sum_{i,j}\overline{\Gamma}^{JT}_{LSMB,N^*_i}(k';E)\mathcal{D}^{-1}_{ij}(E)\overline{\Gamma}^{JT}_{N^*_j,\ell\pi N}(k;E), \quad (6)$$

$$t^{R,JT}_{LSMB,\lambda_\gamma\lambda_N T_{N,z}}(k,q;E) = \sum_{i,j}\overline{\Gamma}^{JT}_{LSMB,N^*_i}(k;E)\mathcal{D}^{-1}_{ij}(E)\overline{\Gamma}^{JT}_{N^*_j,\lambda_\gamma\lambda_N T_{N,z}}(q;E), \quad (7)$$

where the sums $\Sigma_{i,j}$ run over the resonances in a given partial wave (at most two per channel in this work) and $\overline{\Gamma}$ is the dressed vertex function

$$\overline{\Gamma}^{JT}_{LSMB,N^*_i}(k;E) = \Gamma^{JT}_{LSMB,N^*_i}(k) + \sum_{L'S'M'B'}\int dk'\,k'^2 T^{JT}_{LSMB,L'S'M'B'}(k,k';E) \times G_{0,M'B'}(k';E)\Gamma^{JT}_{L'S'M'B',N^*_i}(k') \quad (8)$$

$$\overline{\Gamma}^{JT}_{N^*_i,\lambda_\gamma\lambda_N T_{N,z}}(q;E) = \Gamma^{JT}_{N^*_i,\lambda_\gamma\lambda_N T_{N,z}}(q) + \sum_{LSMB}\int dk\,k^2\overline{\Gamma}^{JT}_{N^*_i,LSMB}(k;E) \times G_{0,MB}(k;E)v_{LSMB,\lambda_\gamma\lambda_N T_{N,a}}(k,q) \quad (9)$$

and $\mathcal{D}^{-1}_{ij}(E)$ is the dressed resonance propagator that depends on the resonance self-energy, $\Sigma_{ij}(E)$:

$$\mathcal{D}_{ij}(E) = \left(E - M^{(0)}_{N^*_i}\right)\delta_{ij} - \Sigma_{ij}(E) \quad (10)$$

$$\Sigma_{ij}(E) = \sum_{LSMB}\int dk k^2\Gamma^{JT}_{N^*_i,LSMB}(k;E)G_{0,MB}(k;E) \times\overline{\Gamma}^{JT}_{LSMB,N^*_j}(k;E). \quad (11)$$

The bare vertex functions Γ should, in principle, be calculated from appropriate *ab initio* hadronic models. This is beyond the scope of the present study. Instead, we parametrize the vertex function in the center-of-mass for the partial wave specified by J, L, S for the hadronic channels as

$$\Gamma^{JT}_{LSMB,N^*}(k) = \zeta_{MB}\frac{1}{(2\pi)^{3/2}}\frac{1}{\sqrt{m_N}}C^{JT}_{N^*LSMB} \times\left(\frac{k}{m_\pi}\right)^L f^{JT}_{N^*LSMB}(k). \quad (12)$$

Here $\zeta_{MB} = -i$ for $MB = \pi N, \eta N, \pi\Delta$ and $\zeta_{MB} = 1$ for $MB = \sigma N, \rho N, \omega N$. At small values of the relative MB

TABLE IV. Lagrangian nonresonant cutoffs (MeV).

$\Lambda_{\pi NN}$	810
$\Lambda_{\pi N\Delta}$	829
$\Lambda_{\rho NN}$	1087
$\Lambda_{\rho\pi\pi}$	1094
$\Lambda_{\omega NN}$	1523
$\Lambda^t_{\omega NN}$	589
$\Lambda_{\eta NN}$	624
$\Lambda_{\sigma NN}$	781
$\Lambda_{\rho N\Delta}$	1200
$\Lambda_{\pi\Delta\Delta}$	600
$\Lambda_{\sigma\pi\pi}$	1200
$\Lambda_{\omega\pi\rho}$	600
$\Lambda_{\rho\Delta\Delta}$	600

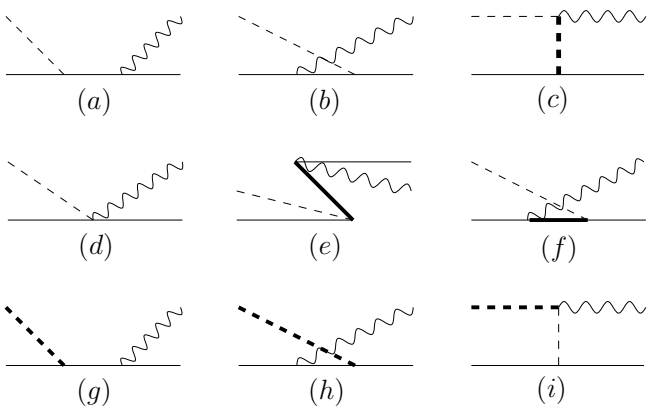

FIG. 4. The $v_{\pi N,\gamma N}$ and $v_{\omega N,\gamma N}$ interaction mechanisms. For photoproduction of π mesons: (a) s-channel nucleon exchange; (b) u-channel nucleon exchange; (c) t-channel π, ρ, and ω exchange; (d) contact interaction; (e) s-channel $\bar{\Delta}$ exchange; (f) u-channel Δ exchange. For photoproduction of ω mesons: (g) s-channel exchange; (h) u-channel exchange; (i) t-channel π exchange.

TABLE V. Bare masses $M^{(0)}$ (MeV) appearing in the resonance propagator of Eq. (5), and the ranges k_{N^*} (MeV), strong couplings G^{JT}_{LSMB,N^*} (MeV$^{-1/2}$) and photocouplings $A^{JT}_{\lambda,p}$ (10^{-3} GeV$^{-1/2}$) in Eqs. (12) and (13).

No.	ℓ_{TJ}	$M^{(0)}$	k_{N^*}	πN	ηN	$\pi\Delta$		σN		ρN			ωN		$A_{\frac{1}{2}}$	$A_{\frac{3}{2}}$
1	S_{11}	1800	99.9	7.049	9.100	−1.853		−2.795	2.028	0.027		−3.761	0.405		83.8	
2	S_{11}	1880	100.0	9.824	0.600	0.045		1.139	−9.518	−3.014		−0.516	0.366		−40.3	
3	S_{31}	1850	20.7	5.275		−6.175			−4.299	5.638					129.4	
4	P_{11}	1763	76.1	3.912	2.621	−9.905		−7.162	−5.157	3.456		−3.362	5.231		−21.8	
5	P_{11}	2037	22.1	9.998	3.661	−6.952		8.629	−2.955	−0.945		−2.095	1.043		−27.5	
6	P_{13}	1711	76.4	3.270	−0.999	−9.988	−5.038	1.015	−0.003	2.000	−0.081	5.737	−0.548	−0.204	−12.4	−63.8
7	P_{31}	1900	100.0	6.803		2.118			9.915	0.153					54.1	
8	P_{33}	1391	−93.3	1.319		2.037	9.538		−0.317	1.036	0.766				−78.6	−131.2
9	P_{33}	1603	83.9	1.312		1.078	1.524		2.012	−1.249	0.379				−6.7	5.3
10	D_{13}	1899	−35.3	0.445	−0.017	−1.950	0.978	−0.482	1.133	−0.314	0.179	−0.081	3.740	0.230	88.8	−71.4
11	D_{13}	1988	−41.7	0.465	0.357	9.919	3.876	−5.499	0.289	9.628	−0.141	7.883	9.900	3.386	−54.5	46.8
12	D_{15}	1898	0.0	0.312	−0.096	4.792	0.020	−0.455	−0.179	1.249	−0.101	0.625	1.086	−0.156	33.0	40.3
13	$\boldsymbol{D_{15}}$	2334	9.7	0.167	−0.106	0.190	−0.098	−0.075	−0.530	0.228	0.099	−0.150	−1.990	0.199	12.6	87.4
14	D_{33}	1976	36.7	0.945		3.999	3.997		0.162	3.949	−0.856				95.9	−6.1
15	F_{15}	2187	92.1	0.062	0.000	1.040	0.005	1.527	−1.035	1.607	−0.026	−0.046	2.212	0.078	−99.8	−68.1
16	F_{35}	2162	−84.2	0.174		−2.961	−1.093		−0.076	8.034	−0.061				−61.0	−103.4
17	F_{37}	2137	−100.0	0.254		−0.316	−0.023		0.100	0.100	0.100				45.9	47.7

momentum k, $\Gamma^{JT}_{LSMB,N^*}(k)$ has the form appropriate to the threshold production behavior, k^L. It is regulated at large k by the form factor, $f^{JT}_{N^*LSMB}(k)$, described below.

The bare electromagnetic coupling for $N^* \to \gamma N$ for all N^* except the first P_{33} resonance (number 8 in Tables V and VI) is given by

$$\Gamma^{JT}_{N^*,\lambda_\gamma\lambda_N T_{N,z}}(q) = \frac{1}{(2\pi)^{3/2}}\sqrt{\frac{m_N}{E_N(q_R)}} \times A^{JT}_{\lambda T_{N,z}}\sqrt{\frac{q_R}{q}}\, g^{JT}_{N^*\lambda T_{N,z}}(q)\,\delta_{\lambda,\lambda_\gamma-\lambda_N}, \quad (13)$$

with $\Gamma^{JT}_{N^*,-\lambda_\gamma,-\lambda_N T_{N,z}} = (-1)^{J+\ell+1/2}\Gamma^{JT}_{N^*,\lambda_\gamma\lambda_N T_{N,z}}$, where N^* is in partial wave ℓ_{JT}. The form for the first P_{33} resonance is shown in the appendix. The photon momentum at the resonance threshold, q_R is $M^{(p)}_{N^*} = q_R + E_N(q_R)$, where $M^{(P)}_N$ is taken from the *Review of Particle Properties* [24]. The isospin projection of the initial nucleon is $T_{N,z}$ and the helicities are λ_γ and λ_N. We assume the forms $f^{JT}_{N^*LSMB}(k) = [{\Lambda^{JT}_{N^*LSMB}}^2/({\Lambda^{JT}_{N^*LSMB}}^2 + (k-k_{N^*})^2)]^{L+2}$ and $g^{JT}_{N^*\lambda T_{N,z}}(q) = 1$. The $C^{JT}_{N^*LSMB}$, $\Lambda^{JT}_{N^*LSMB}$, k_{N^*} and $\mathrm{A}^{JT}_{\lambda T_{N,z}}$ are fit parameters.

III. RESULTS AND DISCUSSION

The first objective of the present study is the simultaneous description of the pion- and photon-induced single-pion and ω-meson production data in a coupled-channels approach. Recent high-precision measurements of ω photoproduction make it possible to strongly constrain coupled-channels model reaction theories. The DCS and ω spin density matrix elements (SDME) have been measured at SAPHIR and published [2] and measured by the CLAS Collaboration [5,25]. The only other measured observable is the single polarization observable, the

TABLE VI. Resonance strong form factor cutoff parameters, $\Lambda^{JT}_{N^*LSMB}$ in MeV.

No.	ℓ_{TJ}	πN	ηN		$\pi\Delta$	σN		ρN			ωN	
1	S_{11}	1676.4	599.0	554.0		801.0	1999.9	1893.7		500.2	817.9	
2	S_{11}	533.5	500.0	1999.1		1849.5	796.8	500.0		503.1	622.0	
3	S_{31}	2000.0		500.0			500.0	500.0				
4	P_{11}	1203.6	1654.8	729.0		1793.1	622.0	1698.9		675.8	516.9	
5	P_{11}	646.9	897.8	501.3		1161.2	500.1	922.3		533.7	950.1	
6	P_{13}	1374.0	500.2	500.0	500.8	640.5	500.0	500.1	1645.2	500.1	547.3	513.3
7	P_{31}	828.8		2000.0			1998.8	2000.0				
8	P_{33}	746.2		846.4	781.0		585.0	500.2	1369.7			
9	P_{33}	880.7		507.3	501.7		606.8	1043.4	528.4			
10	D_{13}	1658.0	1918.2	976.4	1034.5	1315.8	599.8	1615.1	1499.5	565.5	802.9	978.1
11	D_{13}	1094.0	678.4	1960.0	660.0	1317.0	550.1	597.6	1408.7	500.5	506.2	545.2
12	D_{15}	1584.7	1554.0	500.8	820.2	507.1	735.4	749.4	937.5	1036.0	999.2	996.0
13	$\boldsymbol{D_{15}}$	1223.8	1990.2	1910.4	996.1	921.6	1022.0	1941.9	997.0	930.2	998.2	999.2
14	D_{33}	806.0		1359.4	608.1		1515.0	1999.0	956.6			
15	F_{15}	1641.6	655.9	1899.5	522.7	500.9	500.8	500.0	1060.9	541.8	502.0	651.6
16	F_{35}	1035.3		1228.0	586.8		1514.8	593.8	1506.0			
17	F_{37}	1049.0		1180.2	1031.8		600.0	600.0	600.0			

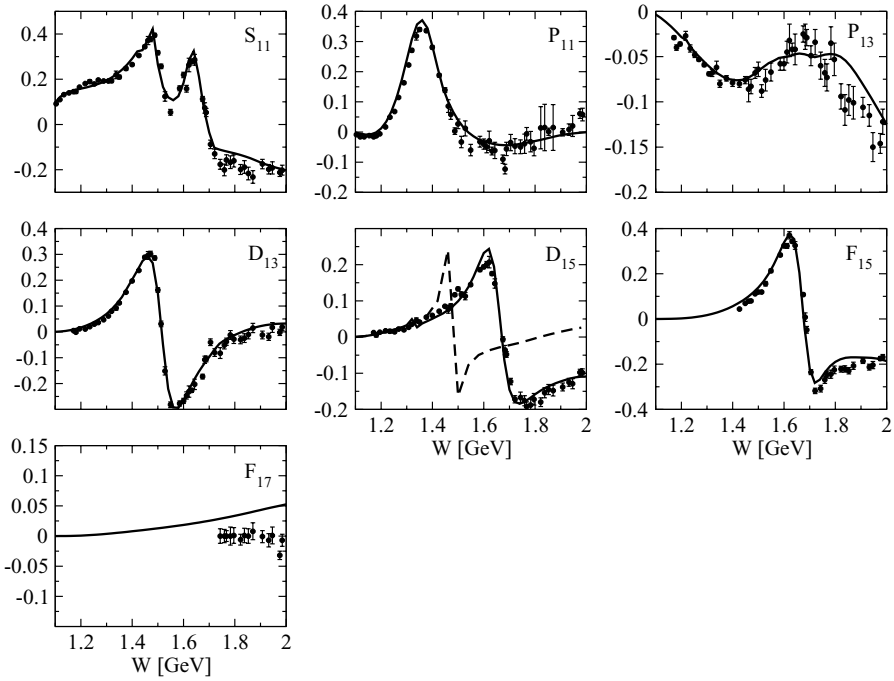

FIG. 5. Real part of $\pi N \to \pi N$ partial wave amplitudes $\overline{T}^{J1}_{\ell\pi N,\ell\pi N}(k_{\pi N}, k_{\pi N}; E = W)$ [Eq. (14)] for $T = 1/2$ versus center-of-mass energy, W (in GeV) by partial wave, $\ell_{2T,2J}$ fit to single energy extraction of Ref. [19]. The dashed line shows the best fit obtained without the second resonance in D_{15}.

photon beam asymmetry (PBA) $\Sigma_\omega(\theta, E)$ at GRAAL [3,4]. We have elected to also include the older π-induced reaction data from threshold ($\sim$1.72 GeV) to 1.764 GeV from the Nimrod synchrotron [7] and the Alvarez detector data from 1.75 to 2.05 GeV [6] (in 100-MeV bins).

The world data for pion photoproduction measurements of DCS, shown in Figs. 10 and 11, and PBA, shown in Figs. 12 and 13, are obtained from the George Washington University Center for Nuclear Studies Data Analysis Center [26]. These high-precision data in $\gamma p \to \pi^0 p$ were taken from Refs. [27–31] for DCS and Refs. [30,33–36] for PBA and in $\gamma p \to \pi^+ n$ from Refs. [28,29,31,32] ([28,30,34–37]) for DCS(PBA), respectively. For the purpose of χ^2 optimization of the data with respect to the bare parameters of the theory a truncated data set of the highest-precision data was used that covers as much of the angular range as was available on a per-energy-bin basis.

To accomplish our objective we take as the starting point for this analysis the T matrix determined in Ref. [38] that fits the $\pi N \to \pi N$ partial-wave amplitudes

$$\overline{T}^{JT}_{\ell\pi N,\ell\pi N}(k_{\pi N}, k_{\pi N}; E) = -\rho_{\pi N}(k_{\pi N}) T^{JT}_{\ell\pi N,\ell\pi N}(k_{\pi N}, k_{\pi N}; E), \qquad (14)$$

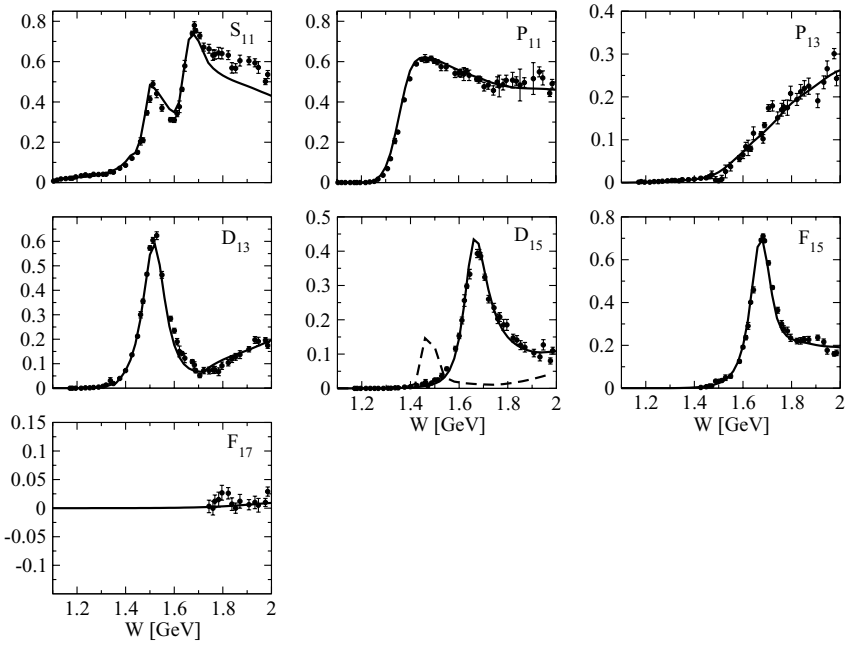

FIG. 6. Imaginary part of $\pi N \to \pi N$ partial wave amplitudes $\overline{T}^{J1}_{\ell\pi N,\ell\pi N}(k_{\pi N}, k_{\pi N}; E = W)$ for $T = 1/2$, as in Fig. 5.

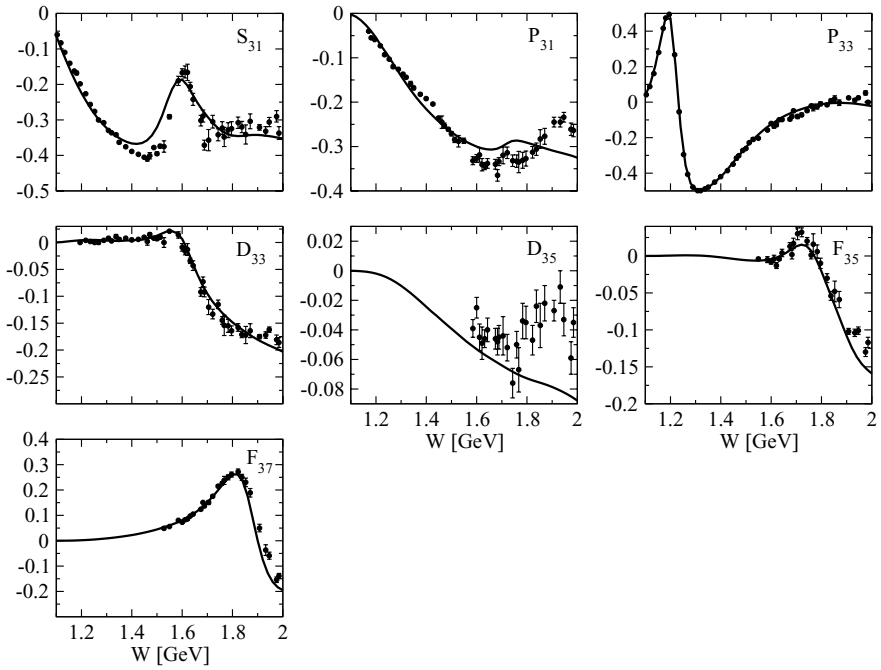

FIG. 7. Real part of $\pi N \to \pi N$ partial wave amplitudes $\overline{T}^{J3}_{\ell\pi N,\ell\pi N}(k_{\pi N}, k_{\pi N}; E = W)$ for $T = 3/2$ versus center-of-mass energy, W (in GeV) fit to single energy extraction of Ref. [19].

extracted from observed data by Ref. [19] in the region 1.1 GeV $< E <$ 2.0 GeV, $E = W$ in a five-channel approach, excluding ωN. The nonresonant parameters determined in Ref. [38] were fixed and are shown in Tables II, III, and IV. The resonance parameters ($M^{(0)}_{N^*}$, $C^{JT}_{N^*LSMB}$, $\Lambda^{JT}_{N^*LSMB}$, and k_{N^*}) for coupling to the five hadronic channels $MB = \pi N, \eta N, \pi\Delta, \sigma N, \rho N$ determined in the fit by Julia-Diaz *et al.* [38] are shown in Tables V and VI.

Determination of the six-channel T matrix $T^{JT}_{LSMB,L'S'M'B'}$ $T^{JT}_{LSMB,\lambda_\gamma\lambda_N T_{N,z}}$ proceeds in two stages. At the first stage, the $\pi N \to \pi N T = 1/2$ partial-wave amplitudes of Figs. 5 and 6, $\pi^- p \to \omega n$ DCS of Fig. 9 and the $\gamma p \to \omega p$ DCS of Fig. 14 are fit simultaneously. (Figures 7 and 8 show the $T = 3/2$ amplitudes, which are unchanged from those of Ref. [38], for completeness.) This is accomplished by adjusting the nonresonant couplings $g^t_{\omega NN}$, $\kappa^t_{\omega NN}$, and $\Lambda^t_{\omega NN}$ appearing in the s- and u-channel ω emission and absorption of Figs. 2(a) and 2(b), Fig. 3, and Figs. 4(g), and 4(h) and by adjusting the resonance parameters $N^* \to \omega N$, $G^{J1}_{N^*LS\omega N}$ and $\Lambda^{J1}_{N^*LS\omega N}$. The introduction of the ωN channel to the calculation requires the addition of a second D_{15} resonance, shown in bold in Tables V and VI, to fit the data. These points will be discussed in more detail below.

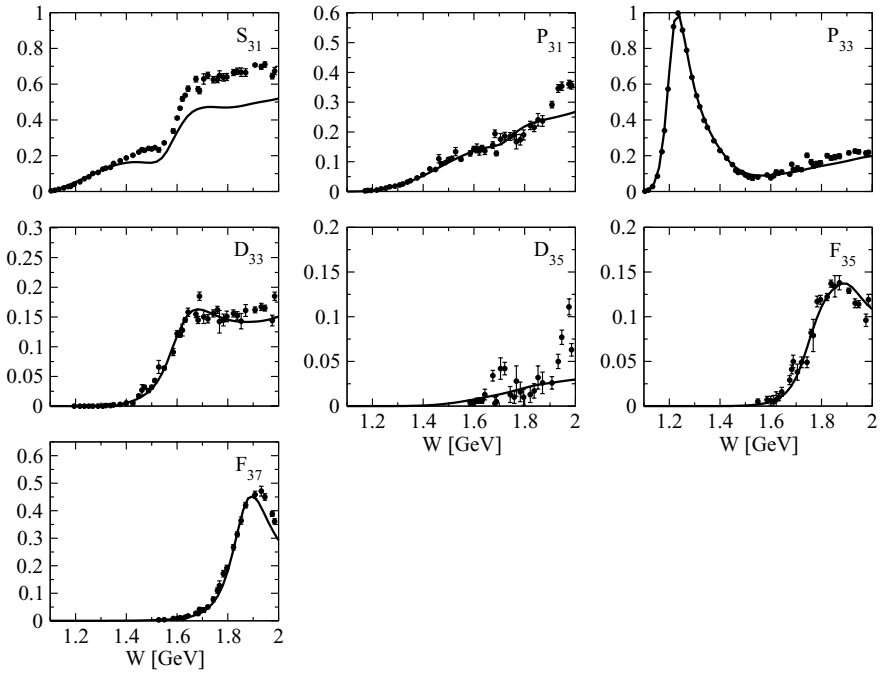

FIG. 8. Imaginary part of $\pi N \to \pi N$ partial wave amplitudes $\overline{T}^{J3}_{\ell\pi N,\ell\pi N}(k_{\pi N}, k_{\pi N}; E = W)$ for $T = 3/2$, as in Fig. 7.

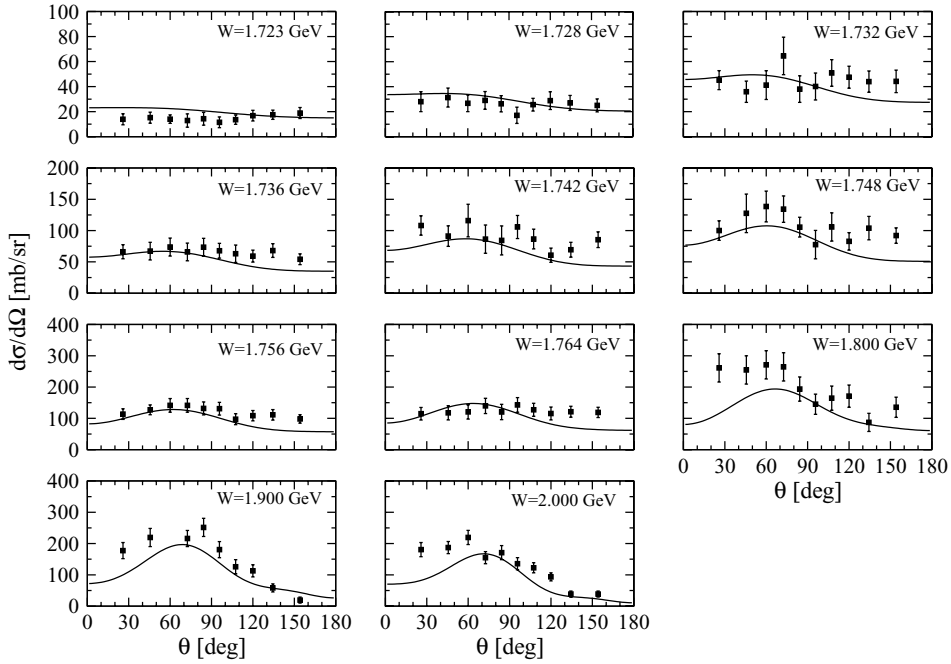

FIG. 9. Differential cross section (in mb/sr) versus center-of-mass angle, θ (in degrees) for $\pi^- p \to \omega n$ compared to data from Refs. [6,7]. The center-of-mass energy, W (in GeV), is shown in each panel.

At the second stage of the fit, all nonresonant and hadronic channel resonant parameters are fixed and the single-meson photoproduction data are fitted. Pion photoproduction data used for the fit include the DCS in Figs. 10 and 11 and the PBA in Figs. 12 and 13 in the region 1.1 GeV $< E <$ 2.0 GeV. ω-meson photoproduction data used for the fit include only the SAPHIR measurement [2] of the DCS from threshold, 1.72 to 2.0 GeV, shown in Fig. 15. This is accomplished by varying the photon helicity couplings, $A^{JT}_{N^*\lambda T_{N,z}}$ for $\lambda = \frac{1}{2}, \frac{3}{2}$ and $T_{N,z} = +\frac{1}{2}$. The resulting fits compared to the existing world data are shown as solid curves in Figs. 10–13.

The overall quality of the fits to the complete set of data are in fair agreement for energies $E < 1.65$ GeV. The $T = 1/2\,\pi N \to \pi N$ partial-wave amplitudes of Fig. 5 agree at the 1- or 2-σ level for all partial waves except the two highest. The $T = 3/2$ partial fits are of similar quality except for the S_{11} wave and the P_{11} wave at energies $E \gtrsim 1.9$ GeV. The fits to the photoproduction data are good at low energies but degrade significantly at $E > 1.65$ GeV, especially in the $\gamma p \to \pi^0 p$ reaction. Coupling to the $\pi\pi N$ channel is expected to be large here.

In contrast to the present study, large values of $g_{\omega NN}$ have been deduced from studies of the nucleon electromagnetic

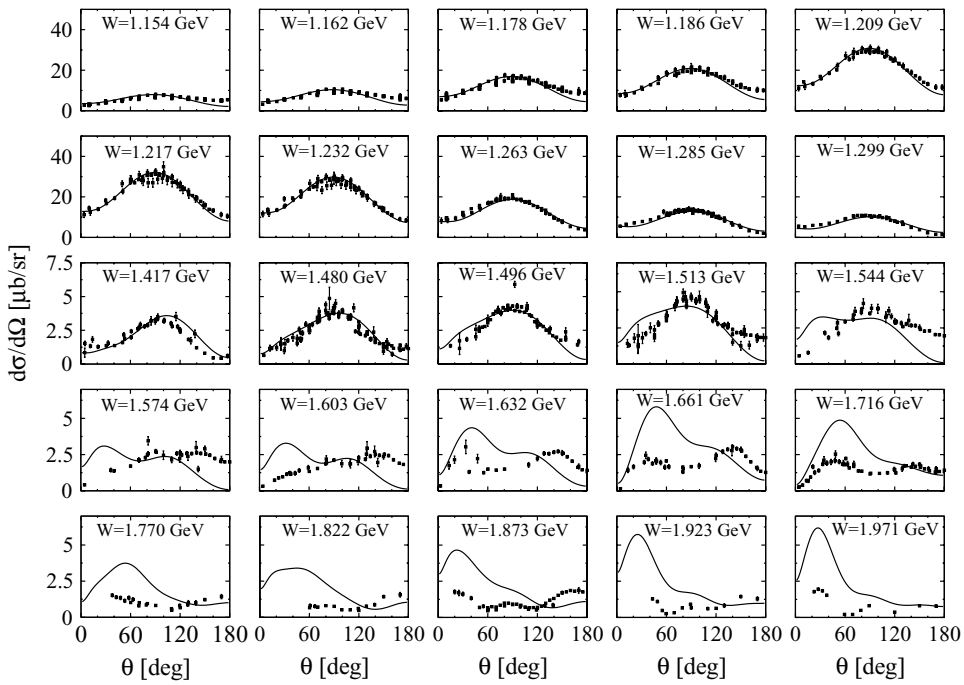

FIG. 10. Unpolarized differential cross section (in μb/sr) versus scattering angle θ (in degrees) in the center-of-mass system for the $\gamma p \to \pi^0 p$ reaction compared to data from Refs. [27–31]. The center-of-mass energy, W (in GeV), is shown in each panel.

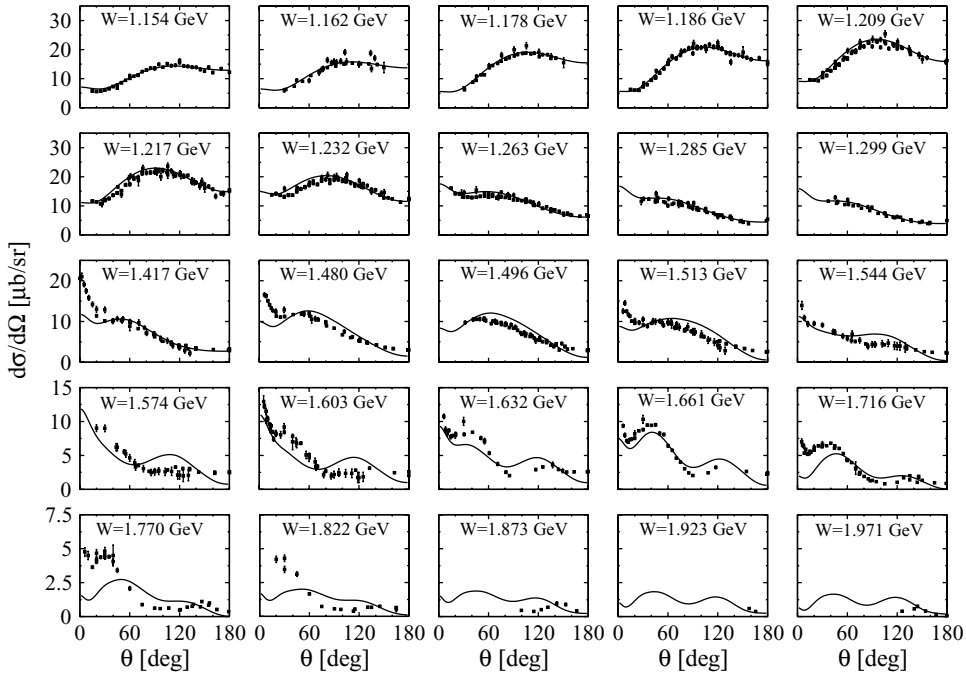

FIG. 11. Unpolarized differential cross section (in μb/sr) versus θ (in degrees) for the $\gamma p \to \pi^+ n$ reaction compared to data from Refs. [28,29,31,32]. The center-of-mass energy, W (in GeV), is shown in each panel.

form factors [39] and various NN studies [40,41]. These studies yield a range of $10 \lesssim g_{\omega NN} \lesssim 20$. Values of this order were assumed for the studies in Ref. [42] though with a strongly suppressing form factor due to a small cutoff, $\Lambda_{\rm OTL} = 0.5$ GeV. At early stages of the fit when we attempted to use the values $g_{\omega NN}$, κ_ω, and $\Lambda_{\omega NN}$ determined in fits to the $\pi N \to \pi N$ data the resulting cross sections were too large by one or two orders of magnitude for both $\pi^- p \to \omega n$ and $\gamma p \to \omega p$ reactions. To fit the data within the present model (keeping the parameters determined in Ref. [38] fixed) for the limited parameter search that we have performed it was necessary to introduce the nonresonant coupling parameters $g^t_{\omega NN}$, κ^t_ω, and $\Lambda^t_{\omega NN}$. These parameters appear at vertices in the graphs of Figs. 2(a) and 2(b), Fig. 3, and Figs. 4(g) and 4(h). A similar situation obtains in $pp \to pp\pi^0$ reactions [43] where different couplings are used for exchanged and emitted s-wave pions. The small value obtained for the coupling $g^t_{\omega NN} \simeq 1.3$ is not too different from the result found by the Giessen group's study [13], $g_{\omega NN} \simeq 4$ (though with different form factors). The treatment here is phenomenological and, as an alternative, one may consider introducing other nonresonant reaction mechanisms involving heavy mesons (e.g., including $v_{\omega N,\rho N}$ or f_0/σ exchange in $v_{\omega N,\pi N}$) or resonances to retain the larger ωNN coupling value. This alternative would provide

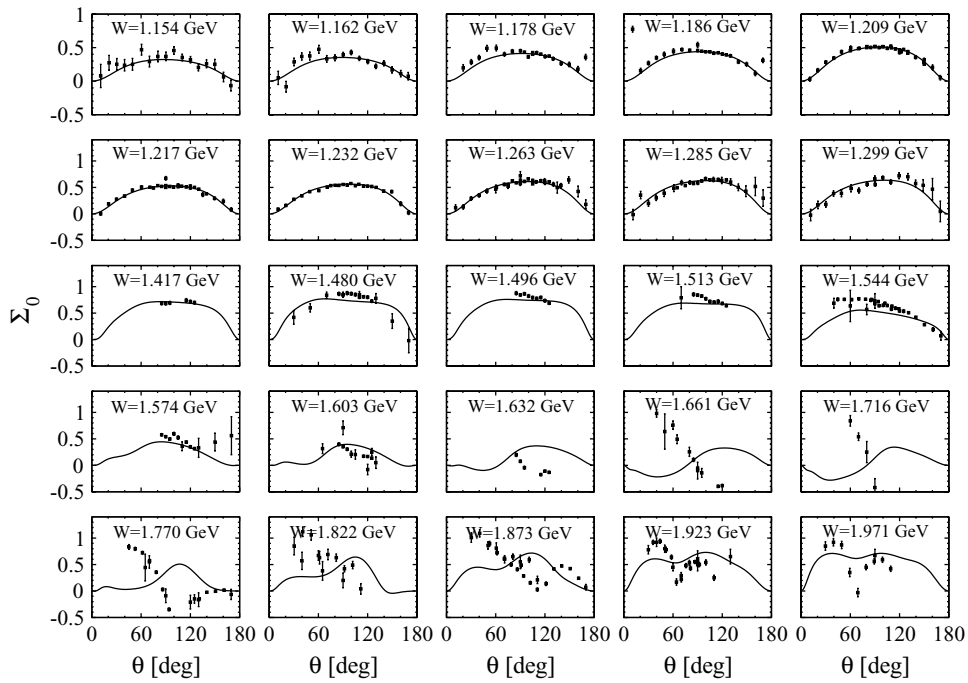

FIG. 12. Photon beam asymmetry $\Sigma_0(\theta, E)$ versus θ (in degrees) for the $\gamma p \to \pi^0 p$ reaction compared to data from Refs. [30, 33–36]. The center-of-mass energy, W (in GeV), is shown in each panel.

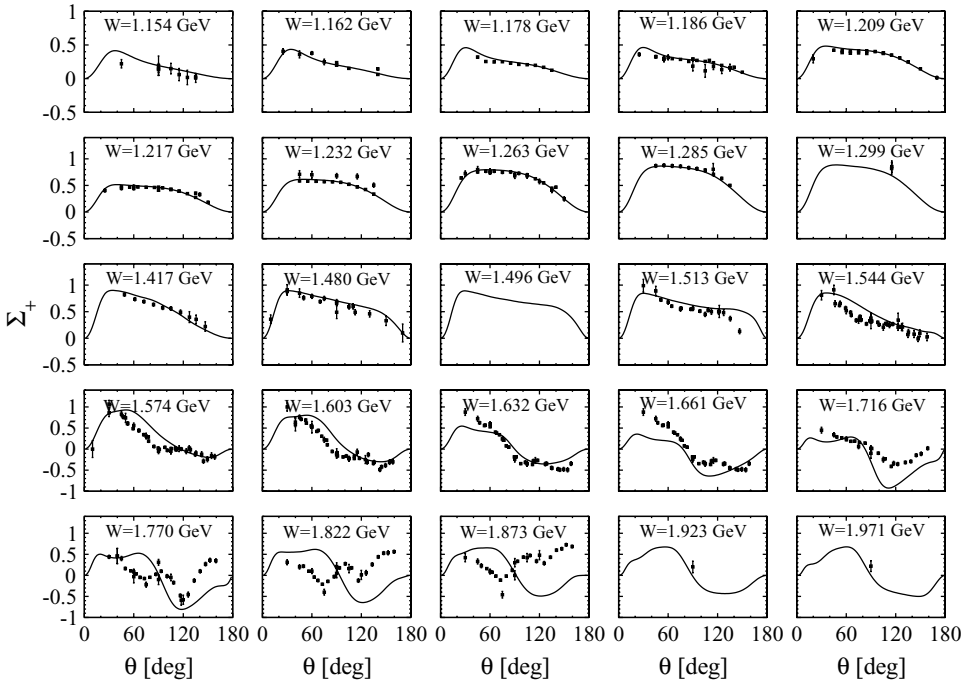

FIG. 13. Photon beam asymmetry, $\Sigma_+(\theta, E)$ versus θ (in degrees) for the $\gamma p \to \pi^+ n$ reaction compared to data from Refs. [28,30,34–37]. The center-of-mass energy, W (in GeV), is shown in each panel.

a guide to the model dependencies of the present approach but within the limited parameter search performed here is beyond the scope of the present study.

Existing hadronic ω production calculations [40,44,45] assume values for the $g_{\omega NN}$ couplings larger than those determined in the present study. It would be interesting to assess, within the context of those models, whether smaller ωNN couplings could be accomodated.

We have found that the introduction of the ωN channel significantly modifies the behavior of the $\pi N \to \pi N D_{15}$ partial-wave amplitude. This is demonstrated in Figs. 5 and 6 where we show as a dashed-line curve in the D_{15} panel the optimal curves found in the first stage fit to $\pi N \to \pi N$, $\pi^- p \to \omega n$, and $\gamma p \to \omega p$ data described above. The $A^{51}_{\frac{3}{2}}$ photocoupling is large and could be an important effect in, for example, the electroproduction reaction. Comparison of the $N^* \to \omega N$ physical masses and branching fractions determined in this work with other calculations (as in Ref. [24]) require the analytic continuation of the T matrix amplitudes to the physical pole position; this work is in preparation.

The prediction for the PBA [46] in $\gamma p \to \omega p$

$$\Sigma_\omega(\theta; E) = \frac{\sigma_\perp - \sigma_{||}}{\sigma_\perp + \sigma_{||}} \tag{15}$$

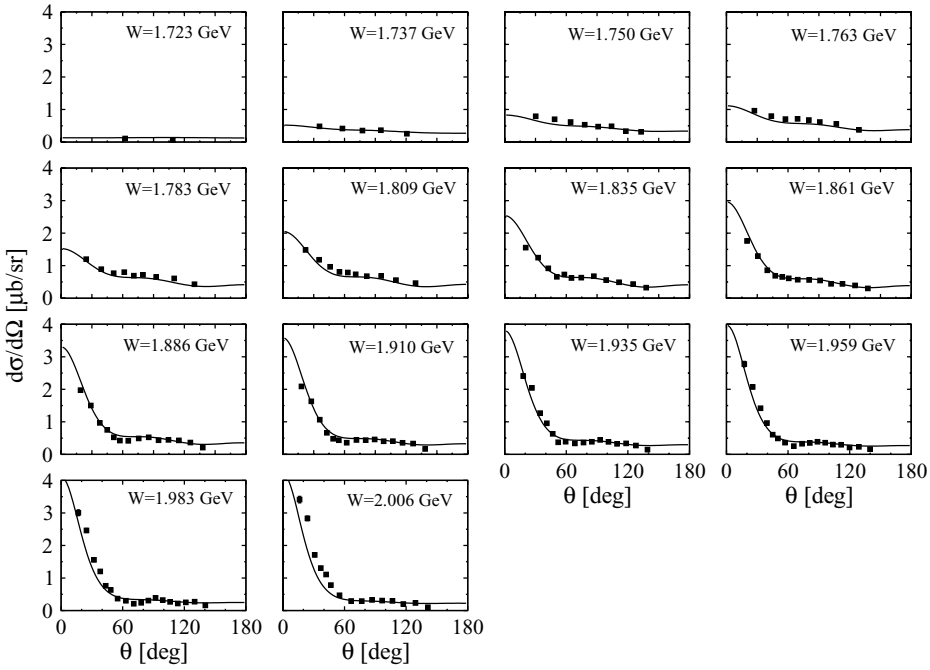

FIG. 14. Unpolarized differential cross section (in μb/sr) for $\gamma p \to \omega p$ versus θ (in degrees) compared to data from Ref. [2]. The center-or-mass energy, W (in GeV), is shown in each panel.

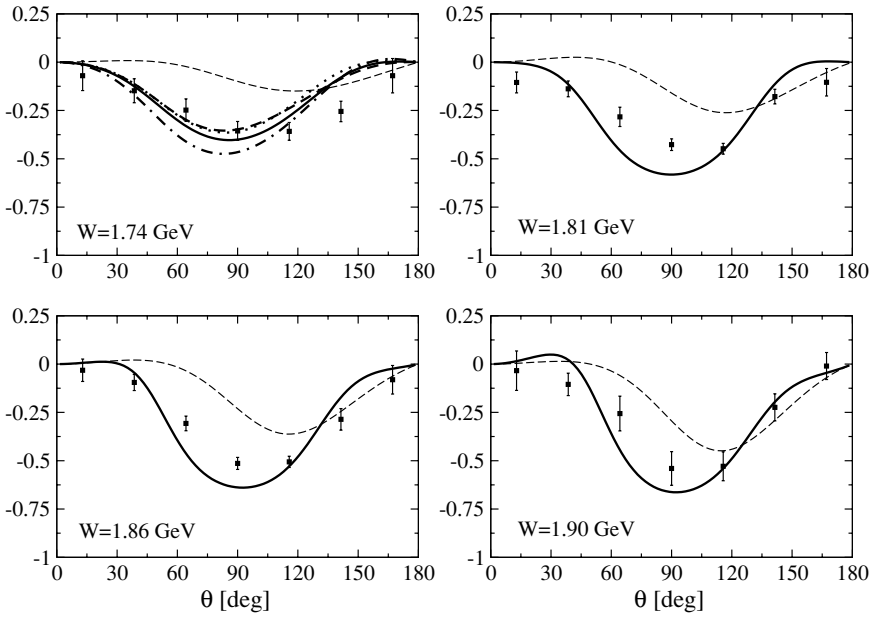

FIG. 15. Predicted photon beam asymmetry, $\Sigma_\omega(\theta, E)$ for $\gamma p \to \omega p$ (solid curve) for $E = W$ shown in each panel compared with data from Ref. [3]. At the lowest energy, the effect of removal of various resonances is shown. Removing all resonance contributions results in the thin dashed curve. Removing the contribution of the resonance partial waves S_{11} (dotted), D_{13} (dashed), or F_{15} (dot-dashed) in turn yields the indicated curves.

is shown in Fig. 15. Here $\sigma_{||}(\sigma_\perp)$ is the differential cross section for linearly polarized photons in (perpendicular to) the emission plane of the ω meson. At the lowest energy $E = 1.743$ GeV a study is made of the sensitivity to the resonance contribution for three cases. The thin-dashed line is the result when all the resonance contributions have been removed. Other curves in the figure show the result when one of three dominant waves is removed.

The total cross section of the reaction $\omega N \to \omega N$ is of interest for realistic calculations of nuclear matter properties. The predicted total cross section for this reaction is shown in Fig. 16. The scattering lengths obtained from the T matrix are

$$a_J = \lim_{E \to m_\omega + m_N} \frac{\pi m_\omega m_N}{m_\omega + m_N} T^J_{0J\omega N, 0J\omega N}(E), \quad (16)$$

$$a_{\frac{1}{2}} = [-0.0454 - i0.0695] \text{ fm}, \quad (17)$$

$$a_{\frac{3}{2}} = [0.180 - i0.0597] \text{ fm}, \quad (18)$$

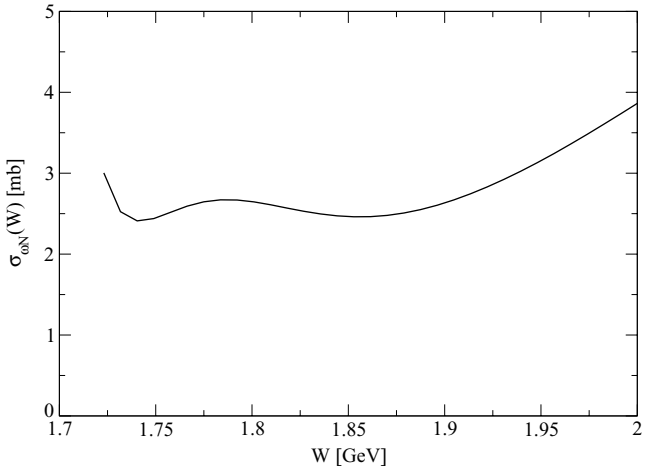

FIG. 16. Calculated total elastic ωN cross section (mb) as a function of center-of-mass energy $E = W$.

related to the total cross section at threshold by $\sigma_{\omega N}(E \to m_\omega + m_N) = 4\pi(|a_{\frac{1}{2}}|^2 + 2|a_{\frac{3}{2}}|^2)/3$.

The total cross section for $\gamma p \to \omega p$ is shown in Fig. 17 along with contributions from partial waves $\ell_{2T,2J}$ with significant contributions. The error bars on the total cross section are statistical [2]. Systematic errors are shown in Ref. [2] to be about 10–15%. They arise from, among other sources, the extrapolation of the DCS in the forward and backward directions for center-of-mass ω-meson scattering angles $\theta < 15^\circ$ and $\theta > 150^\circ$. The systematic errors for the DCS from Ref. [2] are largest in the backward direction where the discrepancy from our calculated cross section, as seen in Fig. 18, is most pronounced. Nevertheless, the present calculated $\gamma p \to \omega p$ DCS appears to miss some small

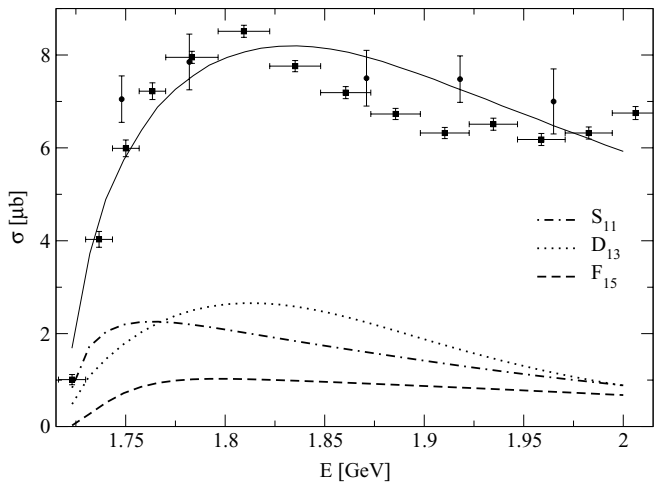

FIG. 17. Total cross section for $\gamma p \to \omega p$ (μb) compared with that extracted from data from Ref. [47] (circles) and Ref. [2] (squares) as a function of center-of-mass energy $E = W$. The error bars on the data from Ref. [2] are statistical errors only. Systematic errors are about 10–15% [2]. The three partial waves with the largest contribution are shown. See the text for discussion.

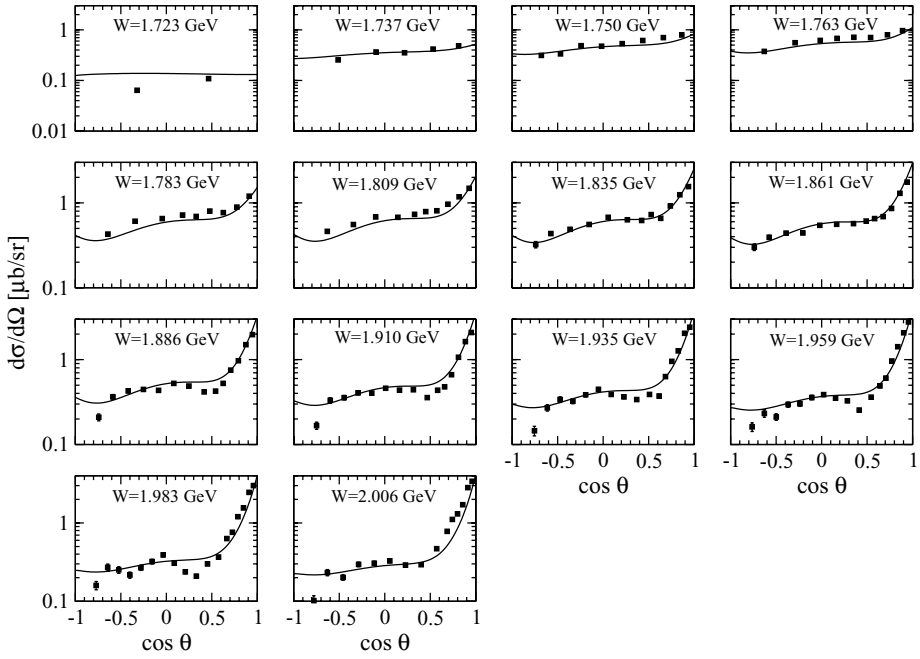

FIG. 18. Semilogarithmic version of Fig. 14, unpolarized DCS for $\gamma p \to \omega p$ (μb/sr) versus $\cos\theta$. Center-of-mass energies are shown in each panel. The sharp angular features are accenuated near $\cos\theta \simeq 0.5$ for $E > 1.86$ GeV and $\cos\theta \simeq -0.5$ for $E \geqslant 1.935$.

angle structure near $\cos\theta \simeq 0.5$ above $E > 1.86$ GeV and $\cos\theta \simeq -0.5$ and 0.5 for $E \geqslant 1.935$ GeV, possibly a result of destructive interference effects of some combination of additional higher mass resonances and nonresonant effects not included in this study.[1]

IV. CONCLUSION

A dynamical coupled-channels model for six channels has been employed in simultaneous fits of the pion- and photon-induced single-pion and ω production reactions. Building on the work of Refs. [1] and [38] we have fixed the parameters of the nonresonant and resonant contributions for the channels πN, ηN, $\pi\Delta$, σN, and ρN for the set of 16 resonances included in Ref. [38]. This model was augmented by including the ωN channel and calculating the nonresonant couplings to the πN channel. We included the resonant contributions for $N^* \to \omega N$ transitions including on-shell and off-shell effects. It was found that an additional, second resonance in the D_{15} partial wave was required to attain a reasonable fit to the extracted amplitude.

Using this model, the parameters have been fixed in χ^2 fits to the πN partial-wave amplitudes and the unpolarized DCS and PBA for pion and ω production reactions for center-of-mass energies from threshold to $W \lesssim 2$ GeV. The results for the πN elastic partial-wave amplitudes are in agreement with the single energy solutions from Ref. [19] up to $W \simeq 2$ GeV for all partial waves considered, excluding the S_{11} and S_{31} that are in agreement with the extracted amplitudes for $W \lesssim 1.7$ GeV. Almost complete agreement with the observed DCS measurements of $\pi^- p \to \omega n$ from Refs. [6,7] except possibly in the energy regions at threshold and near $W \simeq 2$ GeV. For the pion photoproduction data, an excellent reproduction of the observed DCS and PBA is obtained for energies from threshold to $W \simeq 1.5$ GeV. Agreement at higher energies is better for the π^+ production than for π^0 production. Very good agreement with observed ω-meson photoproduction DCS was obtained at all energies considered. However, the present model is in poor agreement with the pion photoproduction data above $W = 1.65$ GeV. However, excellent agreement with the observed DCS for ω production is achieved.

The model was used to predict the PBA in ω production reaction, shown in Fig. 15. The agreement with the data is very good in the forward and backward regions of scattering angle. Near scattering angles of 90°, where resonance contributions are expected to be important, the agreement is not very good.

There are several ways one might attempt to remedy discrepancies with the data. If we work within the present model and keep the same nonresonant mechanisms it is possible that a more thorough search of the parameters may yield a better fit at higher energies. The introduction of more resonances may also yield a better fit. However, for energies $W > 1.8$ GeV the existing data make distinguishing nonresonant mechanisms from resonant mechanisms difficult. Particularly useful in this endeavor would be more high-precision single and double polarization observables for both pion and ω-meson production.

Additional mechanisms in the nonresonant terms are sure to contribute, perhaps significantly, to the calculated scattering observables at these higher energies. At the two-body level we have neglected couplings such as $v_{\omega N,\eta N}$, $v_{\omega N,\pi\Delta}$, $v_{\omega N,\sigma N}$, and $v_{\omega N,\rho N}$. There may also be significant effects from additional mechanisms in the $v_{\omega N,\gamma N}$ interaction. We have neglected the effects of t-channel σ exchange, η exchange (both generally thought to be small), and Pomeron exchange in $\gamma p \to \omega p$, known to have large contributions at forward angles at high energies. At energies above the two-pion production threshold, the $\pi\pi N$-channel contribution can give a significant

[1]This feature is also seen in recent precision data from the CLAS Collaboration [25].

contribution and must be calculated. This can be accomplished in the present model formulation and is currently under study.

ACKNOWLEDGMENTS

The author thanks T. Sato for Born amplitudes, F. Klein and M. Williams for providing data, and T.-S. H. Lee and A. W. Thomas for useful discussions. This work is supported by the US Department of Energy, Office of Nuclear Physics Division, under Contract No. DE-AC02-06CH11357 and Contract No. DE-AC05-060R23177 under which Jefferson Science Associates operates Jefferson Lab. This research used resources of the National Energy Research Scientific Computing Center, which is supported by the Office of Science of the US Department of Energy under Contract No. DE-AC02-05CH11231.

APPENDIX: $P_{33}(1232)$ TRANSITION FORM FACTOR

The transition form factor for $\gamma p \to \Delta(1232)$ is taken as [48]

$$\Gamma^{33}_{\frac{3}{2},p}(q) = -\mathcal{K}_M G_M(q^2) + (\mathcal{K}_M + \mathcal{K}_E) G_E(q^2) \quad \text{(A1)}$$

$$\Gamma^{33}_{\frac{1}{2},p}(q) = \frac{1}{\sqrt{3}}[-\mathcal{K}_M G_M(q^2) + (\mathcal{K}_M - \mathcal{K}_E) G_E(q^2)] \quad \text{(A2)}$$

$$\mathcal{K}_M = \frac{e}{(2\pi)^{3/2}} \sqrt{\frac{E_N(q)+m_N}{2E_N(q)}} \frac{1}{\sqrt{2|q^0|}} \frac{3(m_\Delta + m_N)}{2m_N} \times \frac{E|\mathbf{q}|\sqrt{\pi}}{Q^2 + (m_\Delta + m_N)^2} \quad \text{(A3)}$$

$$\mathcal{K}_E = -\frac{4E|\mathbf{q}|^2}{E_N(q)+m_N} \frac{1}{Q^2 + (m_\Delta - m_N)^2} \mathcal{K}_M. \quad \text{(A4)}$$

On resonance at the photon point, $Q^2 = 0$ the $G_M(0)$ and $G_E(0)$ are related to the value $A^{33}_{\lambda,p}$ in Table V as

$$A^{33}_{\frac{3}{2},p} = -\frac{\sqrt{3}}{2} \frac{e}{2m_N} \sqrt{\frac{m_\Delta |\mathbf{q}|}{m_N}} [G_M(0) + G_E(0)] \quad \text{(A5)}$$

$$A^{33}_{\frac{1}{2},p} = -\frac{1}{2} \frac{e}{2m_N} \sqrt{\frac{m_\Delta |\mathbf{q}|}{m_N}} [G_M(0) - 3G_E(0)]. \quad \text{(A6)}$$

The values in the table correspond to

$$G_M(0) = 1.62 \quad \text{(A7)}$$

$$G_E(0) = 0.015. \quad \text{(A8)}$$

[1] A. Matsuyama, T. Sato, and T. S. H. Lee, Phys. Rep. **439**, 193 (2007).
[2] J. Barth *et al*., Eur. Phys. J. A **18**, 117 (2003).
[3] E. Hourany (GRAAL Collaboration), Nucl. Phys. **A755**, 447 (2005).
[4] J. Ajaka *et al*., Phys. Rev. Lett. **96**, 132003 (2006).
[5] M. Williams, in *Proceedings of the Workshop on the Physics of Excited Nucleons, NSTAR 2005, Florida State University, Tallahassee, USA*, edited by S. Capstick *et al*. (World Scientific Publishing Co., Hackensack, New Jersey, 2006), p. 240.
[6] J. S. Danburg *et al*., Phys. Rev. D **2**, 2564 (1970).
[7] H. Karami *et al*., Nucl. Phys. **B154**, 503 (1979).
[8] C. Hanhart and A. E. Kudryavtsev, Eur. Phys. J. A **6**, 325 (1999).
[9] C. Hanhart, A. Sibirtsev, and J. Speth (private communication, 2001).
[10] S.-N. Yang, J. Phys. G **11**, L205 (1985); S. Nozawa and T. S. H. Lee, Nucl. Phys. A **513**, 543 (1990); C.-C. Lee, S.-N. Yang, and T. S. H. Lee, J. Phys. G **17**, L131 (1991).
[11] O. Krehl, C. Hanhart, S. Krewald, and J. Speth, Phys. Rev. C **62**, 025207 (2000).
[12] G. Y. Chen, S. S. Kamalov, S. N. Yang, D. Drechsel, and L. Tiator, Phys. Rev. C **76**, 035206 (2007).
[13] V. Shklyar, H. Lenske, U. Mosel, and G. Penner, Phys. Rev. C **71**, 055206 (2005).
[14] A. Usov and O. Scholten, Phys. Rev. C **72**, 025205 (2005).
[15] G. E. Brown and M. Rho, Phys. Rev. Lett. **66**, 2720 (1991).
[16] D. Trnka *et al*. (CBELSA/TAPS Collaboration), Phys. Rev. Lett. **94**, 192303 (2005).
[17] P. Muehlich, V. Shklyar, S. Leupold, U. Mosel, and M. Post, Nucl. Phys. **A780**, 187 (2006).
[18] K. Tuchitani *et al*., Int. J. Mod. Phys. E **14**, 955 (2005).
[19] R. A. Arndt, W. J. Briscoe, I. I. Strakovsky, and R. L. Workman, Phys. Rev. C **74**, 045205 (2006).
[20] M. Kobayashi, T. Sato, and H. Ohtsubo, Prog. Theor. Phys. **98**, 927 (1997).
[21] M. Haftel and F. Tabakin, Nucl. Phys. **A158**, 1 (1979).
[22] F. James and M. Roos, Comput. Phys. Commun. **10**, 343 (1975).
[23] T. Sato and T. S. H. Lee, Phys. Rev. C **54**, 2660 (1996).
[24] W. M. Yao *et al*. (Particle Data Group Collaboration), J. Phys. G **33**, 1 (2006).
[25] M. Williams, Ph.D. thesis, Carnegie Mellon University, 2007, http://www-meg.phys.cmu.edu/williams/pdfs/thesis.pdf.
[26] Center for Nuclear Studies (2008), Scattering Analysis Interactive Dial-up, http://gwdac.phys.gwu.edu/.
[27] M. Fuchs *et al*., Phys. Lett. **B368**, 20 (1996); H. Genzel, E. Hilger, G. Knop, H. Kemen, and R. Wedemeyer, Z. Phys. **268**, 43 (1974); P. Argan *et al*., Nucl. Phys. **A237**, 447 (1975); Y. A. Aleksandrov, V. A. Kozlov, and V. V. Pavlovskaya, Yad. Fiz. **28**, 670 (1978); P. Dougan, V. Ramsay, and W. Stiefler, Z. Phys. A **280**, 341 (1977); Y. A. Aleksandrov, V. A. Kozlov, V. N. Maikov, and V. V. Pavlovskaya, Yad. Fiz. **25**, 80 (1977); O. Bartholomy *et al*. (CB-ELSA), Phys. Rev. Lett. **94**, 012003 (2005); Dougan, V. Ramsay, and W. Stiefler, Z. Phys. A **276**, 155 (1976); M. Yoshioka *et al*., Nucl. Phys. **B168**, 222 (1980); Y. Hemmi *et al*., Phys. Lett. **B43**, 79 (1973); R. Worlock, Phys. Rev. **117**, 537 (1960); P. Feller *et al*., Phys. Lett. **B49**, 197 (1974); Y. Hemmi *et al*., Nucl. Phys. **B55**, 333 (1973); J. Ahrens *et al*. (GDH), Phys. Rev. Lett. **88**, 232002 (2002); B. Krusche *et al*., Eur. Phys. J. A **6**, 309 (1999); K. H. Althoff *et al*., Z. Phys. C **1**, 257 (1979); K. H. Althoff *et al*., Zeit. Phys. **C1**, 327 (1979); B. Delcourt, J. Lefrancois, G. Parrour, J. P. Perez-Y-Jorba, and G. Sauvage, Phys. Lett. **B29**, 70 (1969); H. C. DeStaebler, E. F. Erickson, A. C. Hearn, and C. Schaerf, Phys. Rev. **140**, B336 (1965); M. Dugger *et al*., Phys. Rev. C **76**, 025211 (2007); J. S. Barton *et al*., Nucl. Phys. **B84**, 449 (1975); P. S. L. Booth *et al*., Nucl. Phys. **B84**, 437 (1975); L. O. Abrahamian

et al., Sov. J. Nucl. Phys. **23**, 394 (1976); D. Husmann, W. Jansen, B. Lohr, and H. Schilling, Nucl. Phys. **B126**, 436 (1977); W. Brefeld *et al*., Nucl. Phys. **B100**, 93 (1975).
[28] L. O. Abrahamian *et al*., Phys. Lett. **B48**, 463 (1974).
[29] I. Arai *et al*., J. Phys. Soc. Jpn. **43**, 363 (1977).
[30] R. Beck *et al*., Phys. Rev. Lett. **78**, 606 (1997).
[31] J. Ahrens *et al*. (GDH and A2 Collaboration), Eur. Phys. J. A **21**, 323 (2004).
[32] G. Fischer *et al*., Nucl. Phys. **B16**, 119 (1970); G. Fischer, G. Von Holtey, G. Knop, and J. Stuempfig, Z. Phys. **253**, 38 (1972); K. Buechler *et al*., Nucl. Phys. **A570**, 580 (1994); D. Branford *et al*., Phys. Rev. C **61**, 014603 (1999); T. Fujii *et al*., Nucl. Phys. **B120**, 395 (1977); T. Fujii *et al*., Phys. Rev. Lett. **26**, 1672 (1971); H. W. Dannhausen *et al*., Eur. Phys. J. A **11**, 441 (2001); C. Betourne, J. C. Bizot, J. P. Perez-y Jorba, D. Treille, and W. Schmidt, Phys. Rev. **172**, 1343 (1968); Y. M. Aleksandrov, V. F. Grushin, E. M. Leikin, and A. Y. Rotvain, Yad. Fiz. **12**, 770 (1970); J. L. Faure *et al*., Nucl. Phys. **A424**, 383 (1984); K. H. Althoff *et al*., Z. Phys. C **18**, 199 (1983); S. D. Ecklund and R. L. Walker, Phys. Rev. **159**, 1195 (1967); J. Ahrens *et al*., Phys. Rev. C **74**, 045204 (2006) ; K. Ekstrand, A. Browman, L. Hand, and M. E. Nordberg, Phys. Rev. D **6**, 1 (1972); R. A. Alvarez, G. Cooperstein, K. Kalata, R. C. Lanza, and D. Luckey, Phys. Rev. D **1**, 1946 (1970); L. Y. Zhu *et al*. (Jefferson Lab Hall A Collaboration), Phys. Rev. C **71**, 044603 (2005); G. Buschhorn, J. Carroll, R. D. Eandi, P. Heide, R. Hübner, W. Kern, U. Kötz, P. Schmüser, and H. J. Skronn, Phys. Rev. Lett. **17**, 1027 (1966).
[33] G. Blanpied *et al*. (LEGS Collaboration), Phys. Rev. Lett. **69**, 1880 (1992); A. A. Belyaev *et al*., Nucl. Phys. **B213**, 201 (1983); G. Barbiellini *et al*., Phys. Rev. **184**, 1402 (1969); F. V. Adamian *et al*., Phys. Rev. C **63**, 054606 (2001); P. J. Bussey *et al*., Nucl. Phys. **B104**, 253 (1976).
[34] G. Knies *et al*., Phys. Rev. D **10**, 2778 (1974).
[35] P. J. Bussey *et al*., Nucl. Phys. **B154**, 492 (1979).
[36] G. Blanpied *et al*., Phys. Rev. C **64**, 025203 (2001).
[37] V. N. Zabaev *et al*., Yad. Fiz. **21**, 551 (1975); R. C. Smith and R. F. Mozley, Phys. Rev. **130**, 2429 (1963); R. E. Taylor and R. F. Mozley, Phys. Rev. **117**, 835 (1960); V. B. Ganenko *et al*., Yad. Fiz. **23**, 310 (1976); V. A. Getman *et al*., Nucl. Phys. **B188**, 397 (1981); J. Ajaka *et al*. (GRAAL Collaboration), Phys. Lett. **B475**, 372 (2000); J. Alspector *et al*., Phys. Rev. Lett. **28**, 1403 (1972).
[38] B. Julia-Diaz, T. S. H. Lee, A. Matsuyama, and T. Sato, Phys. Rev. C **76**, 065201 (2007).
[39] G. Hohler *et al*., Nucl. Phys. **B114**, 505 (1976).
[40] K. Nakayama, A. Szczurek, C. Hanhart, J. Haidenbauer, and J. Speth, Phys. Rev. C **57**, 1580 (1998).
[41] R. Machleidt, K. Holinde, and C. Elster, Phys. Rep. **149**, 1 (1987).
[42] Y.-s. Oh, A. I. Titov, and T. S. H. Lee, Phys. Rev. C **63**, 025201 (2001).
[43] D. S. Koltun and A. Reitan, Phys. Lett. **141**, 1413 (1966); M. E. Schillaci, R. R. Silbar, and J. E. Young, Phys. Rev. **179**, 1539 (1969); G. A. Miller and P. U. Sauer, Phys. Rev. C **44**, R1725 (1991); T. S. H. Lee and D. O. Riska, Phys. Rev. Lett. **70**, 2237 (1993).
[44] C. Fuchs, M. I. Krivoruchenko, H. L. Yadav, A. Faessler, B. V. Martemyanov, K. Shekhter, Phys. Rev. C **67**, 025202 (2003).
[45] K. Tsushima and K. Nakayama, Phys. Rev. C **68**, 034612 (2003).
[46] A. I. Titov, Y.-s. Oh, S. N. Yang, and T. Morii, Phys. Rev. C **58**, 2429 (1998).
[47] F. J. Klein (SAPHIR Collaboration), PiN Newslett. **14**, 141 (1998).
[48] H. F. Jones and M. D. Scadron, Ann. Phys. **81**, 1 (1973).